JGR Space Physics

RESEARCH ARTICLE
10.1029/2024JA033701

Key Points:

- We statistically study the response of electric field pulses and particle dynamics to the enhanced P_{dyn} under varied IMF directions
- The generation of electric field pulses shows a day-night asymmetry especially under southward IMF
- Proton flux variations cluster on the post-dawnside, while electron flux changes show a weaker tendency to concentrate on the pre-duskside

Supporting Information:

Supporting Information may be found in the online version of this article.

Correspondence to:

X. Gao,
gaoxl@ustc.edu.cn

Citation:

Zhou, X., Gao, X., Lu, Q., Hajra, R., & Ma, J. (2025). Response of electric field pulse and particle dynamics in Earth's magnetosphere to enhanced solar wind dynamic pressure with varied IMF directions: A statistical study. *Journal of Geophysical Research: Space Physics*, *130*, e2024JA033701. https://doi.org/10.1029/2024JA033701

Received 31 DEC 2024
Accepted 27 JUN 2025

Response of Electric Field Pulse and Particle Dynamics in Earth's Magnetosphere to Enhanced Solar Wind Dynamic Pressure With Varied IMF Directions: A Statistical Study

Xuan Zhou[1,2], Xinliang Gao[1,2], Quanming Lu[1,2], Rajkumar Hajra[1,2], and Jiuqi Ma[1,2]

[1]Deep Space Exploration Laboratory, School of Earth and Space Sciences, University of Science and Technology of China, Hefei, China, [2]CAS Center for Excellence in Comparative Planetology, Hefei, China

Abstract The electric field pulses caused by enhanced solar wind dynamic pressure are particularly effective in energization and inward transport of relativistic electrons in Earth's radiation belt. Utilizing electric field and particle measurements by Van Allen Probes and near-Earth solar wind measurements, we have conducted a statistical analysis to investigate the responses of electric field pulses and particle dynamics to enhanced solar wind dynamic pressure under varied interplanetary magnetic field (IMF) directions. On Earth's dayside, the generation of electric field pulses is independent of the IMF direction. In contrast, on the nightside, electric field pulses are more easily excited under northward IMF than under southward IMF. Interacted with the electric field pulses, the responses of electrons and protons show a day-night asymmetry under southward IMF. The statistical results also indicate that proton flux variations mostly cluster on the post-dawnside (MLT ∼ 6–12), while electron flux variations show a slight preference for the pre-duskside (MLT ∼ 12–18) under some conditions. Moreover, the occurrence rate of proton flux variation is lower than that of electrons, and a clear change in proton flux usually appears in lower energy channels. Our study provides new insights into understanding the interaction between solar winds and magnetospheres of the Earth and other magnetized planets.

1. Introduction

The interaction between solar winds and Earth's magnetosphere predominantly governs the dynamic evolution of Earth's near-space environment. Specifically, upon the impact of the solar wind with enhanced dynamic pressure on the Earth's magnetosphere, a series of phenomena are induced, including the compression of the magnetopause (Chapman & Ferraro, 1931; Sibeck et al., 1991), the generation of global electric field pulses (Kim et al., 2009; Knott et al., 1985; Shinbori et al., 2004; Wygant et al., 1994), the generation of magnetopause-ionosphere currents (Nishimura et al., 2016; Samsonov et al., 2010; Zesta et al., 2000; Zhou & Tsurutani, 1999), the occurrence of magnetic reconnection, and the emergence of wave disturbances (Usanova et al., 2008; Fu et al., 2012; N. Liu et al., 2017, 2018). Our primary focus here is on the induced global electric field pulses, which are initially excited at the dayside magnetopause and then azimuthally propagate toward the nightside (Kim et al., 2009; Takahashi et al., 2017; Zhang et al., 2022). The electric field pulses can effectively energize and inward transport relativistic electrons, thereby causing a significant enhancement in the relativistic electron population in Earth's radiation belt (Blake et al., 1992; Foster et al., 2015; Kanekal et al., 2016; Schiller et al., 2016; Wygant et al., 1994). Satellite observations also showed that these pulses can lead to electron depletion in the radiation belt (Hao et al., 2016; Z. Y. Liu et al., 2017, 2019). The response of electron fluxes is determined by the radial gradient of electron phase space density (PSD). When the PSD gradient is positive (negative), the inward transport of electrons by the electric field pulses leads to an enhancement (depletion) in electron fluxes (Cohen et al., 2019; Ma et al., 2021).

The characteristics of electric field pulses are principally regulated by solar wind dynamic pressure. The temporal profile of the electric field pulses correlates with that of the solar wind dynamic pressure, and the pulse amplitude increases with the rising solar wind dynamic pressure (Zhang et al., 2018). However, the formation mechanism of electric field pulses is still under debate. Some studies suggested that their appearance is linked to fast-mode waves excited by the compression of Earth's dayside magnetosphere (Araki et al., 1997; Cattell et al., 2017; Foster et al., 2015; Takahashi et al., 2017). Other studies suggested that the electric field pulses are caused by the motion of plasma flow due to magnetosphere compression triggered by the passage of an interplanetary shock (Fathy et al., 2018; Kim et al., 2009, 2012). Zhang et al. (2022), based on satellite observations and simulations, proposed that the electric field pulses are caused by the superposition effect of the fast-mode waves and the

motion of plasma flow related to the magnetosphere compression, which is more likely to account for the observational outcomes. In any case, both mechanisms have demonstrated the important role of magnetospheric compression caused by enhanced dynamic pressure in the generation of electric field pulses.

Previous studies have shown that the magnetosphere compression caused by enhanced solar wind dynamic pressure varies in accordance with the orientation of the interplanetary magnetic field (IMF). When the IMF is northward, the geomagnetic fields usually undergo compression at all local times (Lee & Lyons, 2004; Zuo et al., 2015). In contrast, during southward IMF conditions, the dayside geomagnetic fields experience compression, while the nightside magnetic fields may decrease or exhibit dipolarization-like changes (Lee & Lyons, 2004; Wang et al., 2009). Simulations further support that an interplanetary shock under a southward IMF will lead to a strong and wide region of decreased geomagnetic fields in the nightside (Sun et al., 2011). These disparate responses of magnetosphere compression under different IMF directions prompt us to investigate whether the electric field pulse and resultant particle flux enhancement or depletion are influenced by the IMF direction.

In this study, utilizing electric field and particle measurements by Van Allen Probes along with near-Earth solar wind measurements, we conduct superposed epoch analyses to investigate the response of electric field pulses to the enhanced solar wind dynamic pressure under varying IMF orientation. Since electric field pulses can effectively interact with particles, we then investigate the corresponding response of electrons and protons from 100 s keV to relativistic energies. The instruments onboard Van Allen Probes and data processing methods are described in Section 2. The statistical results are presented in Section 3. Finally, we summarize and discuss the statistical results in Section 4.

2. Data Sources and Methods

2.1. Data Sources

The Van Allen Probes mission, composed of two identical spacecraft, was initially put into use on 30 August 2012. They operate in near-equatorial orbits with a perigee of about 600 km, an apogee of 30,500 km, and a flight period of 9 hr. The Electric Field and Waves instrument (EFW) (Wygant et al., 2013) onboard Van Allen Probes can provide the y-component of electric fields in the modified Geocentric Solar Ecliptic (MGSE) coordinate system at a sampling rate of 32 per s. The Electric and Magnetic Field Instrument Suite and Integrated Science (EMFISIS) (Kletzing et al., 2013) instrument measured background magnetic fields at low-resolution (64 Hz). The Magnetic Electron Ion Spectrometer (MagEIS) incorporated in the Energetic Particle, Composition, and Thermal Plasma (ECT) suite (Spence et al., 2013) provided the fluxes of electrons and protons from ∼30 keV to relativistic energy (MeV). The Relativistic Electron-Proton Telescope (REPT) yielded electron fluxes from 1.8 MeV to 10 s MeV. High-resolution (1-min) near-Earth solar wind measurements shifted to the Earth's bowshock nose were obtained from the OMNIWeb database (http://spdf.gsfc.nasa.gov/pub/data/omni/). Geomagnetic SYM-H index data (1-min resolution) were obtained from the World Data Center for Geomagnetism, Kyoto, Japan (https://wdc.kugi.kyoto-u.ac.jp/).

2.2. Methods

Magnetospheric compression by sudden increases in the solar wind dynamic pressure leads to electric field pulses and sharp increases in SYM-H, the latter being known as the sudden impulses (SI^+s; Araki et al., 1993; Tsurutani & Lakhina, 2014; Tsurutani et al., 2011). Thus, pulse events are identified using the SYM-H index temporal variations from 1 October 2012 to 31 December 2017 when Van Allen Probes measurements were available. Following Jin et al. (2022), we define a pulse event as a rapid increment in SYM-H values surpassing 5 nT (ΔSYM-H) within 5 min and exclude events without corresponding solar wind dynamic pressure changes. For each selected event, if the average value of IMF in 10 min prior to the SYM-H increase is negative, it is classified as a "southward IMF pulse"; otherwise, it is classified as a "northward IMF pulse." The observations from Van Allen Probes A and B are utilized to study the response of the electric fields and particle fluxes for these pulse events. To eliminate overlapping measurements, observations from two satellites within a 1-hr Magnetic Local Time (MLT) interval are processed as a single measurement. Moreover, we also exclude the measurements where the satellites were located in the trough region or inner radiation belt due to the sparse occurrence of electric field pulses and stable particle fluxes within these regions. Consequently, we collect 278 validated measurements from

the two satellites for the following analyses. Since the geomagnetic fields are more sensitive to enhanced solar wind dynamic pressure, the detrended magnetic fields (the difference between the observed fields and the International Geomagnetic Reference Fields) are employed to determine the zero epoch time in the superposed epoch analyses. The zero epoch time is defined as the time when the detrended magnetic fields begin to increase or decrease at a rate of 1 nT/min, accompanied by a cumulative magnetic field variation exceeding 3 nT. If the variation in the detrended geomagnetic fields is negligible, the zero epoch time is set as 1 min after the SYM-H index rises. We finally examine the flux responses of electrons (0.1–5.6 MeV; 21 energy channels) and protons (0.1–1.2 MeV; 16 energy channels) to quantify the resultant particle dynamics induced by the SYM-H pulse. Here, multi-energy-channel particle flux analysis is used to mitigate possible miscalculations arising from the zero gradient of particle PSD in a single channel. If the average flux of electrons and protons in the 2 min following the zero epoch time either increases or decreases by at least 15% in at least two adjacent energy channels compared with the fluxes at the zero epoch time, it is considered that the electron and proton fluxes effectively respond to the SYM-H pulse events. Otherwise, they are regarded as having no perceptible response or an ambiguous response (the oscillation of particle fluxes obscures the response to enhanced SYM-H) to the SYM-H pulse events. Particles with energies in the tens of keV range are excluded due to their close correlation with substorm activity, and cases where the variation of particle flux is caused by satellite movement are also excluded.

Figure 1 shows examples of the electric field pulse events and particle responses to enhanced solar wind dynamic pressure under southward and northward IMF conditions. During the interval of southward IMF (Figure 1a, shaded in gray), an enhanced dynamic pressure (Figure 1b) impinging on the Earth's magnetosphere instigated a sudden pulse (SI^+) in the SYM-H index from 10 to 38 nT (Figure 1c) at 05:45 UT on 22 June 2015. Nearly simultaneously, Van Allen Probe B, located on the dayside of Earth (MLT ∼16.4), observed a sharp increase in the detrended geomagnetic field from −5 to 15 nT (Figure 1d) and a decrease in the *y*-component of the electric field from 0 to −3 mV/m (Figure 1f). The peak of the electric field pulse was directed towards the dawnside, which interacts with the drifted electrons, leading to the enhancement of ∼100 keV–2.6 MeV electron fluxes (Figures 1f and 1g). During this interval, proton fluxes exhibited no significant changes (Figure 1h).

Figures 1i–1p present another example under northward IMF conditions. Compression of the Earth's magnetosphere by the enhanced dynamic pressure (Figure 1j) led to an increase in the SYM-H index from ∼20 to 65 nT (Figure 1k) at 04:46 UT on 17 March 2015. Slightly later, Van Allen Probe B, located on the nightside of Earth (MLT ∼20.3), detected a sharp increase in the detrended magnetic field from ∼−25 to 0 nT (Figure 1l) and an increase in the electric field from 0 to 6 mV/m (Figure 1m). The peak of this electric field pulse, directed towards the duskside, corresponded to an enhancement of electron fluxes in the 100–600 keV range and a decrease in electron fluxes above 600 keV (Figures 1n and 1o). This differential response originates from energy-dependent electron PSD gradients (Turner et al., 2012). Specifically, high-energy electrons in this region exhibit negative PSD gradients, while low-energy electrons display positive gradients, leading to the observed increase in electron fluxes at lower energies and decrease at higher energies. In this case, proton fluxes also did not undergo significant changes (Figure 1p).

3. Statistical Results

We categorize the selected events into three groups based on the SI^+ amplitude (SYM-H increase): ΔSYM-H < 10 nT, 10 ≤ ΔSYM-H < 20 nT, and ΔSYM-H ≥ 20 nT. Separate analyses are conducted for dayside and night cases in each group. Figure 2 presents the superposed epoch analysis results of the detrended geomagnetic field and *y*-component of the electric field in response to enhanced solar wind dynamic pressure under northward (left panels) and southward (right panels) IMFs on the Earth's dayside for three categories. The red and dark blue lines denote the mean and median values, respectively. The detrended magnetic and electric fields are normalized by subtracting the value at the zero epoch time. Note that the detrended magnetic field is shown only as a reference for event onset and is not the focus of the subsequent analysis. Figure 2b reveals that under northward IMF, even a weak increase in solar wind dynamic pressure (ΔSYM-H < 10 nT) can induce significant electric field pulses. As ΔSYM-H increases, the amplitude of the electric field pulses also increases (Figure 2, left panels), reaching up to 2 mV/m for ΔSYM-H ≥ 20 nT (Figure 2f). Under southward IMF (Figure 2, right panels), for ΔSYM-H < 10 nT (Figure 2h), the electric field response is scarcely distinguishable, presumably due to the limited number of events (only six). For ΔSYM-H ≥ 10 nT (Figures 2j and 2l), electric field pulses appear with amplitudes and temporal evolutions similar to those under northward IMF. This suggests that the generation of electric field pulses on the Earth's dayside is independent of the IMF direction.

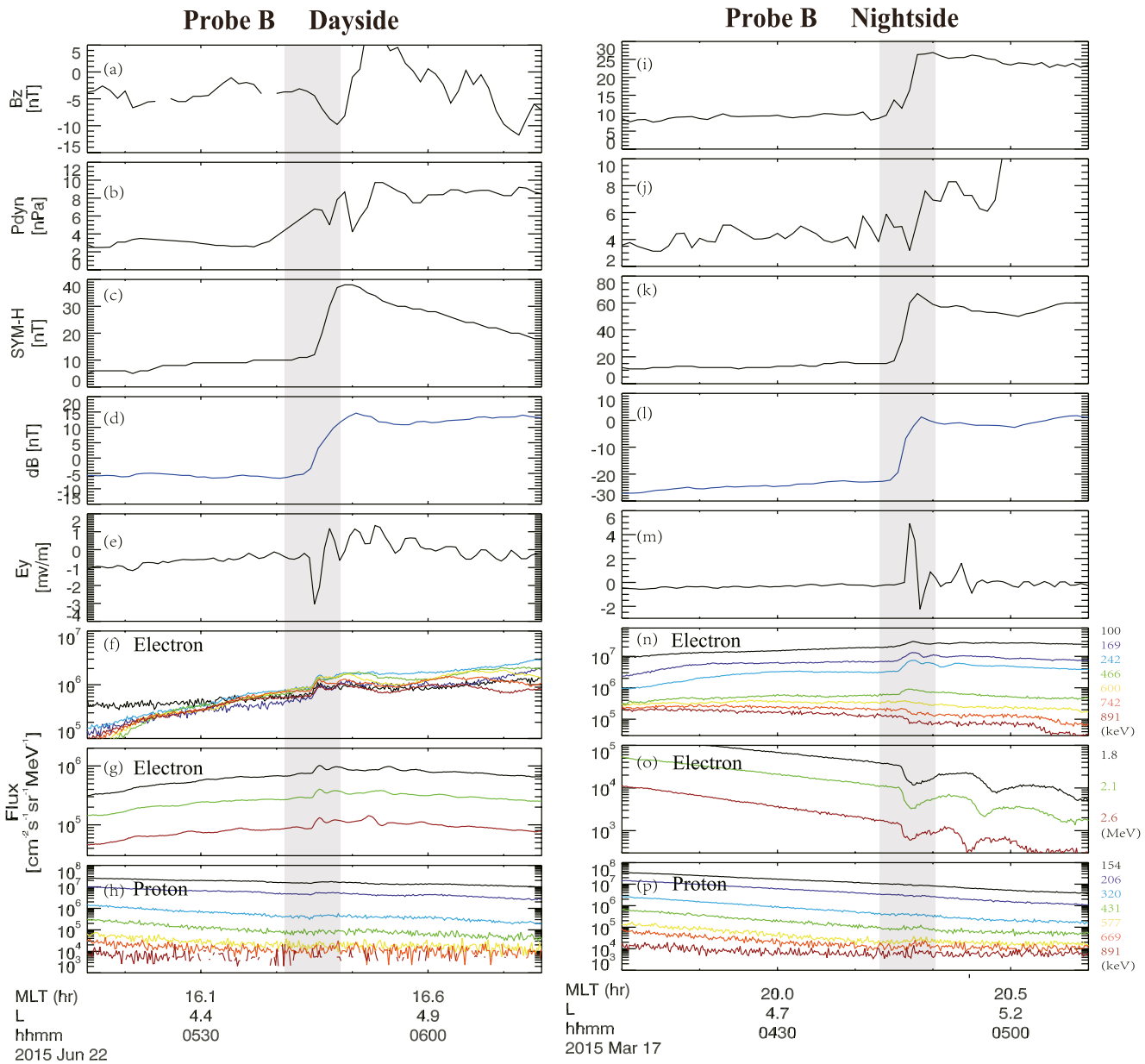

Figure 1. Overview of the response of electric field pulse and particle fluxes to the enhanced solar wind dynamic pressure under southward IMF (a–h) and under northward IMF (i–p). From top to bottom, panels are: (a, i) B_z component of the interplanetary magnetic field in the geocentric solar magnetospheric (GSM) coordinate system, (b, j) solar wind dynamic pressure (P_{dyn}), (c, k) SYM-H index, (d, l) detrended geomagnetic field (dB) recalculated by subtracting the International Geomagnetic Reference Field (IGRF), (e, m) 40-s averaged y-component of electric field (E_y) in the Modified Geocentric Solar Ecliptic (MGSE) coordinate system, (f, n) fluxes of electrons with energy 100, 169, 242, 466, 600, 742, and 891 keV, (g, o) fluxes of electrons with energy 1.8, 2.1, and 2.6 MeV, (h, p) fluxes of protons with energy 154, 206, 320, 431, 577, 669, and 891 keV.

Figure 3 presents the superposed epoch analysis results on the Earth's nightside under northward (left panels) and southward (right panels) IMFs. Under northward IMF, the response of the electric field to a weak increase in solar wind dynamic pressure is negligible (Figure 3b). For $10 \leq \Delta$SYM-H < 20 nT (Figure 3d), the electric field pulse becomes discernible, with its amplitude reaching 0.5 mV/m. With a further increase of ΔSYM-H (Figure 3f), the amplitude of the electric field pulse rises to 1 mV/m. Under southward IMF, a weak increase in solar wind dynamic pressure fails to cause significant changes in the electric field (Figure 3h). For $10 \leq \Delta$SYM-H < 20 nT (Figure 3j), electric field pulses still remain untriggered by the enhancement of solar wind dynamic pressure. Instead, the electric field intensity gradually increases, attaining its peak nearly 5 min after the zero epoch time.

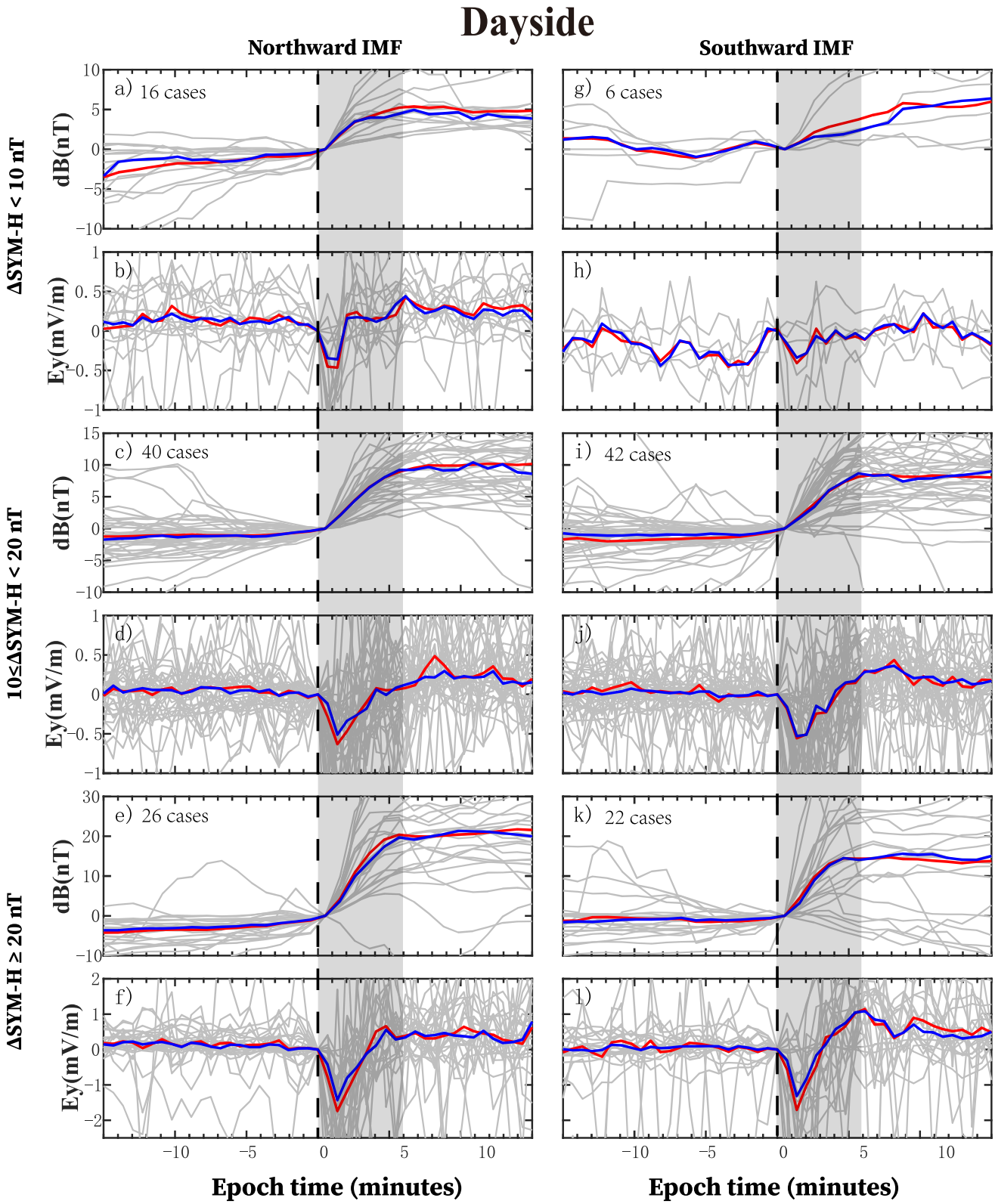

Figure 2. The superposed epoch analysis of the detrended geomagnetic field (dB) and *y*-component of electric field (E_y) in response to the enhanced solar wind dynamic pressure under the northward IMF (a–f) and southward IMF (g–l) on the Earth's dayside for ΔSYM-H < 10 nT, 10 ≤ ΔSYM-H < 20 nT and Δ SYM-H ≥ 20 nT. The red and dark blue lines represent the mean and median values.

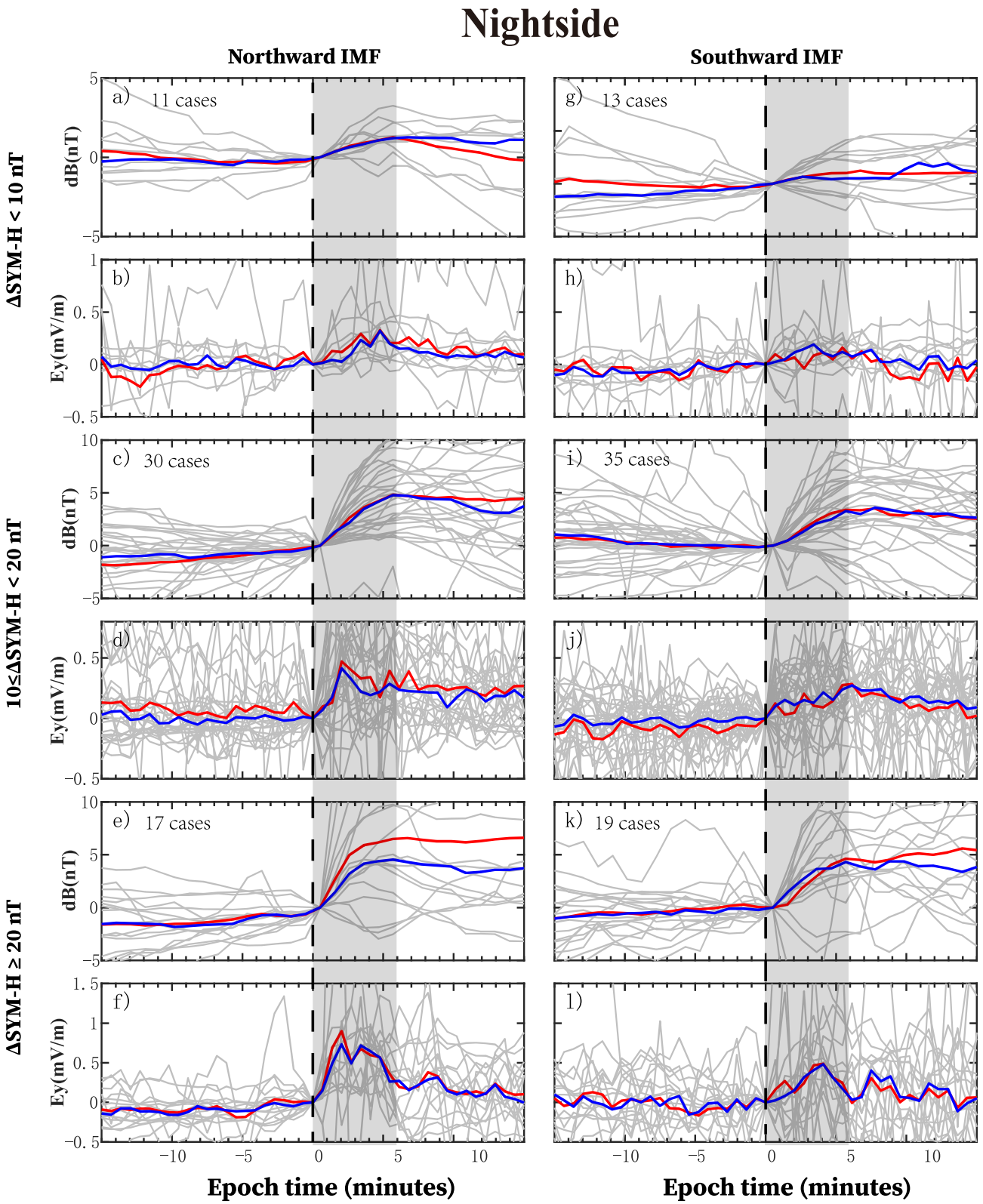

Figure 3. The superposed epoch analysis results of the detrended geomagnetic field (dB) and *y*-component of electric field (E_y) in response to the enhanced solar wind dynamic pressure under the northward IMF (a–f) and southward IMF (g–l) on the Earth's nightside. The panels are in the same format as in Figure 2.

We propose that this elevation in electric field intensity might be associated with storm- or substorm-related electric fields. For ΔSYM-H ≥ 20 nT (Figure 3l), the electric field pulses emerge, however, their amplitudes are smaller than under northward IMF. In comparison to northward IMF, the enhancement of solar wind dynamic pressure under southward IMF is less effective in inducing the electric field pulses on the Earth's nightside. The electric field pulses manifest significant day-night asymmetry, especially under southward IMF. This day-night asymmetry was also noted by Zhang et al. (2018), but they ignored the effect of IMF orientation.

The induced electric field pulses can effectively interact with electrons, leading to flux enhancements or depletions in Earth's radiation belt. We conduct a statistical study of electron responses under different IMF conditions to investigate how the enhancement of solar wind dynamic pressure affects electron flux via induced electric field pulses. We also study proton responses in our analysis, although they have received relatively less attention in previous studies. Figures 4a–4c display electron responses under northward IMF for ΔSYM-H < 10 nT, 10 ≤ ΔSYM-H < 20 nT, and ΔSYM-H ≥ 20 nT, respectively. Figures 4d–4f present the results under southward IMF in the same format. Red circles denote effective responses of particle fluxes to SYM-H pulses, while blue squares and gray triangles represent no perceptible and ambiguous responses of particle fluxes to SYM-H pulses, respectively. The ratio of the number of red circles to the total number of red circles and blue squares (e.g., occurrence rate of particle flux variations) on different MLT ranges is noted around the periphery of the MLT-L plane (L is the McIlwain's drift-shell parameter, representing the distance (in Earth radii) for a dipole magnetic field line to cross the magnetic equatorial plane; McIlwain, 1961). Figure 4 shows that, for a particular IMF orientation, the electron fluxes are more prone to change when the enhancement of ΔSYM-H is more significant. This aligns with the superposed epoch analysis results, showing that electric field pulses are more easily induced by the more dramatic enhancement of ΔSYM-H.

Under northward IMF (Figures 4a–4c), the electron response does not exhibit significant asymmetry between the Earth's dayside and nightside. However, under southward IMF (Figures 4d and 4e), electron responses exhibit significant day-night asymmetry, especially for ΔSYM-H > 10 nT. On the Earth's dayside (6 < MLT < 18), the difference in occurrence rates of electron flux variations between northward and southward IMFs is negligible: around 51% (18/35) versus ∼53% (20/38) for 10 ≤ ΔSYM-H < 20 nT and 84% (21/25) versus ∼86% (18/21) for ΔSYM-H ≥ 20 nT. On the nightside (MLT < 6 and MLT > 18), the occurrence rate of electron flux variations under northward IMF is remarkably higher than that under southward IMF: around 46% (12/26) versus 28% (7/25) for 10 ≤ ΔSYM-H < 20 nT and 85% (17/20) versus ∼53% (9/17) for ΔSYM-H ≥ 20 nT.

Figure 5 shows the response of protons under northward and southward IMF in the same format as in Figure 4. Generally, the behavior of proton responses is similar to that of electrons. Their fluxes are more inclined to change with significant enhancements of ΔSYM-H, and display a day-night asymmetry under southward IMF. However, the occurrence rate of proton flux variation is lower than that of electrons. For example, regardless of any conditions, the occurrence rate of electron flux variations is ∼53% (132/251), while that of protons is only ∼31% (81/264). By examining our database, we also find that the typical change of electron fluxes can be observed in the energy channel up to several MeV, while the clear change of proton fluxes only appears in the energy channel below 1 MeV, with an average value of 442 keV. Another notable phenomenon is that electron flux variations in response to the SYM-H pulses mostly cluster on the Earth's duskside, while proton flux variations mostly cluster on the dawnside, especially for 10 ≤ ΔSYM-H < 20 nT. As shown in Figures 4b and 4e, the occurrence rates of electron flux variations on the pre-duskside (12 < MLT < 18) are higher than those on the post-dawnside (6 < MLT < 12): around 68% (15/22) versus ∼23% (3/13) under northward IMF and 60% (12/20) versus ∼44% (8/18) under southward IMF. The occurrence rates of proton flux variations on the dawnside are higher than that on the duskside: around 43% (6/14) versus 28% (7/25) under northward IMF and around 53% (9/17) versus ∼26% (6/23) under southward IMF (Figures 5b and 5e). These differences are caused by the different drift directions of protons and electrons around the Earth, which will be discussed in detail later. In summary, both protons and electrons are effectively transported by the induced electric field, and their responses also relate to the direction of the IMF.

4. Conclusions and Discussion

In this study, utilizing the data from the Van Allen Probes and Omni database from 1 October 2012 to 31 December 2017, we statistically study the response of electric field pulses to the enhanced solar wind dynamic pressure under northward and southward interplanetary magnetic fields (IMFs). Since the electric field pulses can

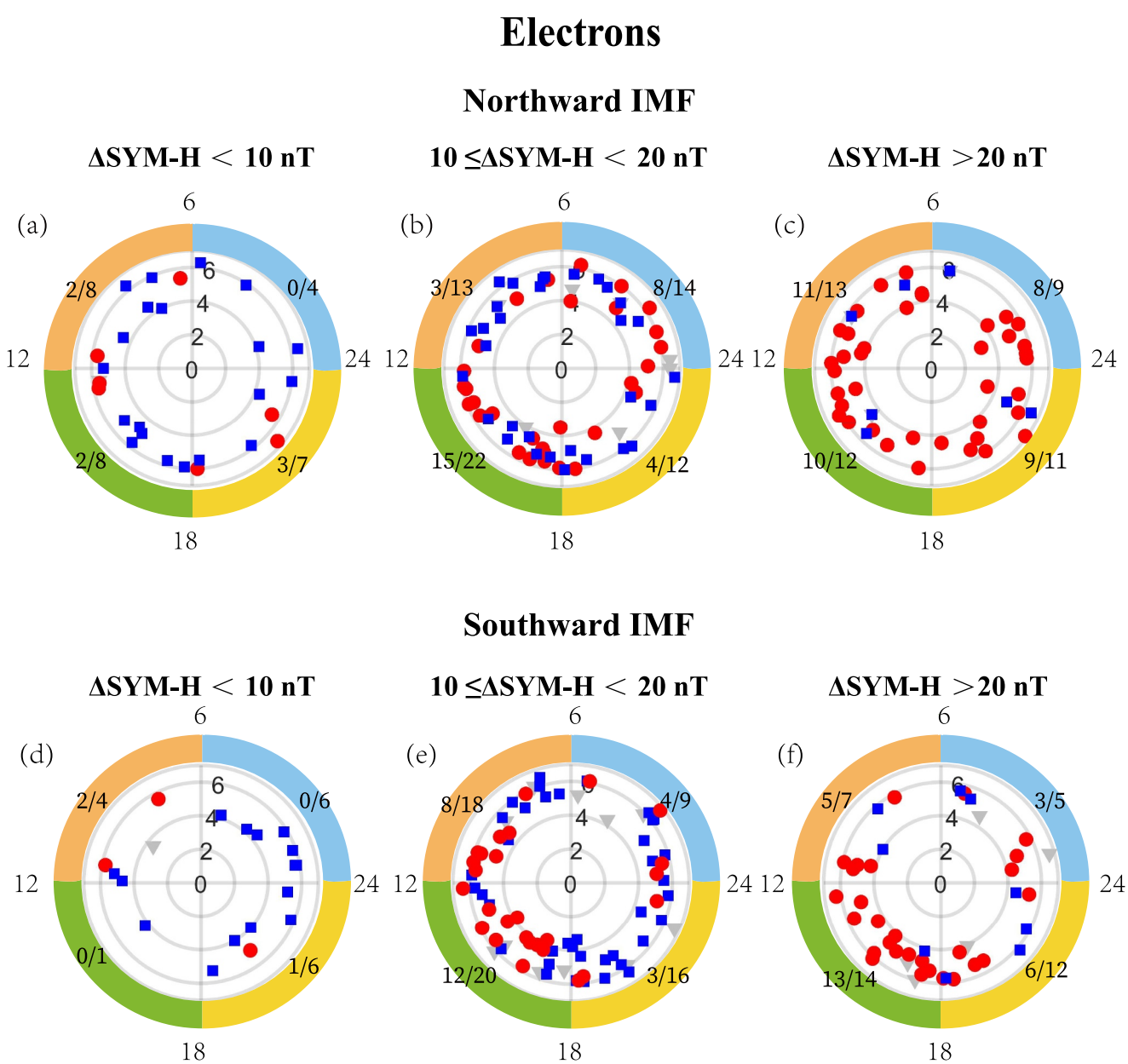

Figure 4. The response of electrons to the enhanced solar wind dynamic pressure under northward IMF (a–c) and southward IMF (d–f) for ΔSYM-H < 10 nT, 10 ≤ ΔSYM-H < 20 nT, and ΔSYM-H ≥ 20 nT in the MLT-L coordinates. Red circles denote effective responses of particle fluxes to SYM-H pulses, while blue squares and gray triangles represent no perceptible and ambiguous responses to SYM-H pulses, respectively. The ratio of the number of red circles to the total number of red circles and blue squares (e.g., occurrence rate of particle flux variations) on different MLT ranges are noted around the periphery of the MLT-L plane.

interact with charged particles effectively, we also investigate the corresponding response of electrons from 0.1 to 5.6 MeV and protons from 0.1 to 1.2 MeV. The principal results are listed as follows:

1. The generation of electric field pulses on the Earth's dayside is independent of the IMF direction, while on the nightside, the electric field pulses are more easily excited under northward IMF than under southward IMF. There exists a day-night asymmetry of electric field pulses, especially under southward IMF.
2. The responses of electrons and protons are more significant when the enhancement of solar wind dynamic pressure is larger, and their responses also show a day-night asymmetry under southward IMF.
3. The occurrence rate of proton flux variations is significantly lower than that of electrons. Moreover, a typical change in electron fluxes can be observed in the energy channel up to several MeV, while a clear change in proton fluxes usually appears in lower energy channels below 1 MeV.

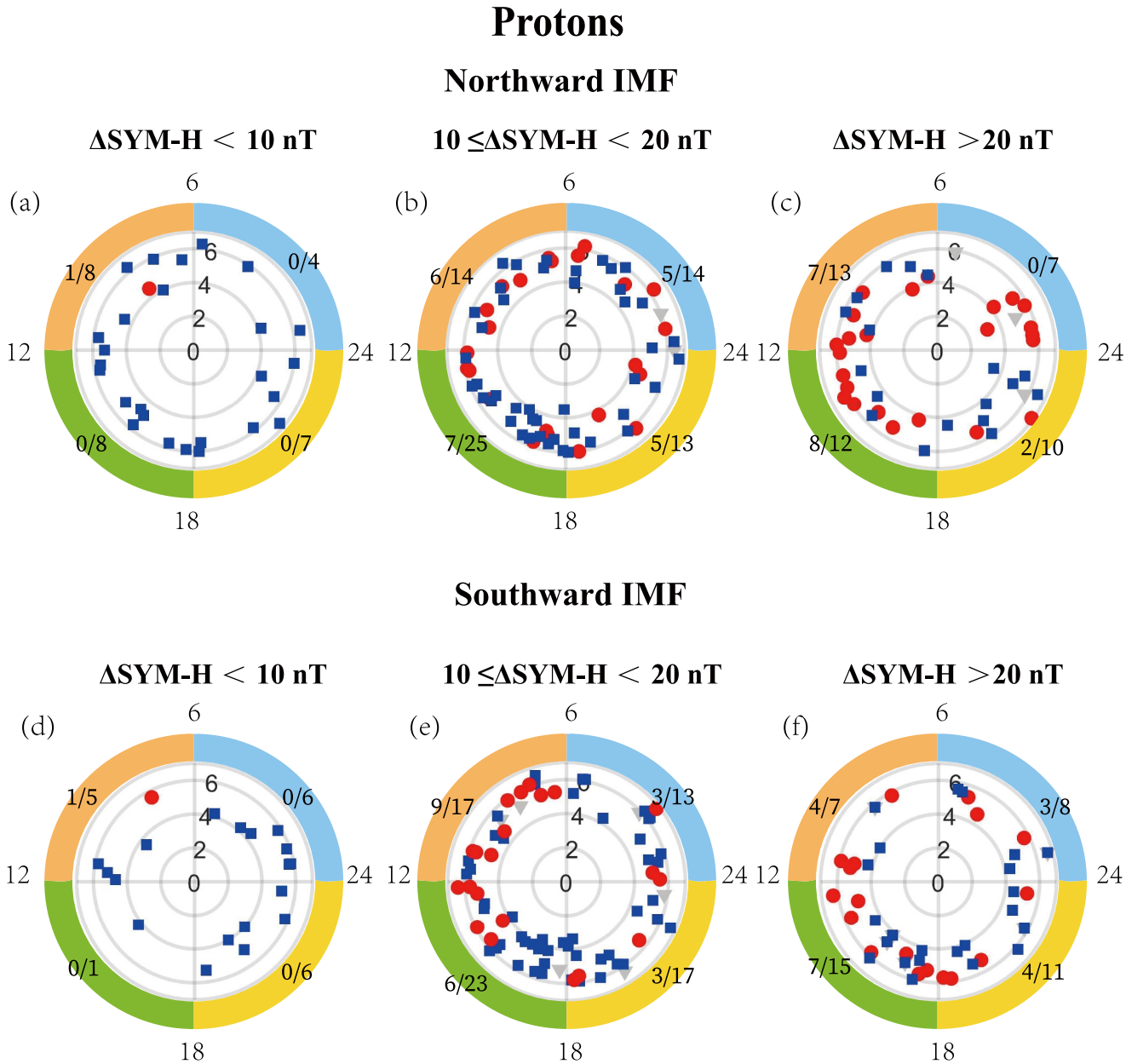

Figure 5. The response of protons to the enhanced solar wind dynamic pressure. The format is the same as in Figure 4.

4. Proton flux variations primarily cluster on the post-dawnside (MLT ~ 6–12), while electron flux variations exhibit a weaker tendency to concentrate in the pre-duskside (MLT ~ 12–18) under some conditions.

Simulations and observational studies have indicated that the generation of electric field pulses is linked to fast-mode waves and the motion of plasma flow instigated by magnetospheric compression (Zhang et al., 2022). As fast-mode waves progress in the tailward direction, they should experience a successive attenuation. Concurrently, the velocity of solar wind decelerates as they move from the subsolar region to the magnetotail, leading to the weakening of the magnetospheric compression. Accordingly, the electric field pulse undergoes a continuous weakening during its propagation, thereby resulting in the day-night asymmetry of the electric field pulses.

On the Earth's nightside, electric field pulses are principally correlated with the plasma flow arising from magnetospheric compression. In the presence of a southward IMF, the enhanced solar wind dynamic pressure can trigger dayside magnetic reconnection, which may cause a larger plasma sheet current (Kan, 1990). A larger

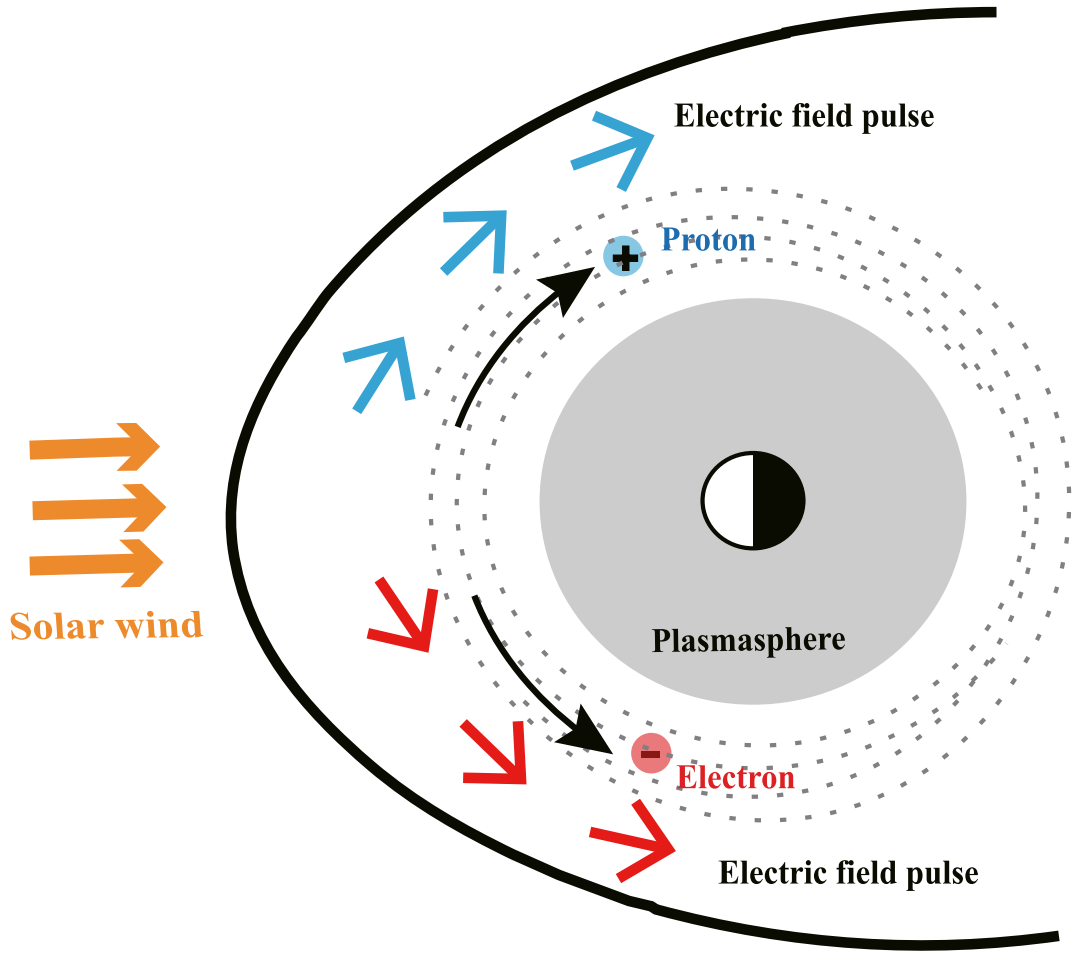

Figure 6. Schematic diagram of electric field pulse propagation and particle drifts. The blue and red arrows show the propagation directions of the electric field pulses on the dawnside, and duskside, respectively. The black arrows show the drift directions of protons and electrons.

plasma sheet current may lead to the weaker compression of nightside magnetic fields or even a decline in magnetic field strength on Earth's nightside, consequently causing a weaker induced electric field. Therefore, nightside electric field pulses are less likely to appear under southward IMF than under northward IMF, explaining a more pronounced day-night asymmetry of the electric field pulses under southward IMF.

Our study reveals that the occurrence rate of proton flux variation is lower than that of electrons, and the clear change of proton fluxes usually appears in lower energy channels. Based on the observed temporal scales of electric field pulses (~5 min) and the estimated propagation velocities (from ~850 to over 1,000 km/s; Foster et al., 2015; Cattell et al., 2017), we calculate that the spatial scale of electric field pulses ranges from ~255,000 to over 300,000 km, significantly exceeding the gyroradius of electrons and protons. Consequently, the differential gyroradius between ions and electrons fails to elucidate their different responses as both species undergo an inward drift. We further propose that the significantly lower occurrence rate of proton flux variations compared to that of electrons is potentially caused by the smaller PSD gradient of protons. When particles are transported toward Earth by the electric field pulse, the particle fluxes with the same energy detected by the satellite are not the same group as the particles observed before transportation, but from a larger L* (Ma et al., 2021). This implies that the electron PSD profile with L* determines the variations in particle fluxes observed by the satellite. If the PSD gradient of the proton approaches zero, the satellite will detect no flux variations. Based on the observations from Van Allen Probes, we statistically study the PSD radial profiles for protons and electrons in January 2014 under the T89 magnetic model (Tsyganenko, 1989). The superposed epoch analysis results are presented in Figure S1. Figure S1 reveals that protons exhibit smaller PSD gradients compared to electrons, and the magnitude of proton PSD gradients decreases with proton energy. This result

agrees with our observations that protons are less responsive than electrons, with the proton flux changes predominantly confined to lower energies.

The different drift directions of protons and electrons determine the spatial difference in their flux variation regions. As shown schematically in Figure 6, following the impact of enhanced solar wind dynamic pressure, the electric field pulse is initially induced near the subsolar point and then propagates towards both dawnside and duskside (Zhang et al., 2022, 2024). On the duskside, electrons drift in the same direction as the electric field pulses, and the electrons can sustain interaction with the electric field pulses over a longer period and gain more energy. In contrast, on the dawnside, protons drift in the same direction as the propagation of electric field pulses, facilitating sustained interaction and increased energy gain. Consequently, proton flux variations mostly cluster on the post-dawnside (MLT ~ 6–12), while electron flux variations show a slight preference for the pre-duskside (MLT ~ 12–18).

Data Availability Statement

The RBSP data used in this study are available from the website https://spdf.gsfc.nasa.gov/pub/data/rbsp/. The omni data are obtained from the website http://spdf.gsfc.nasa.gov/pub/data/omni/.

Acknowledgments
This research was funded by the NSFC Grants 42322406 and 42230201, the "USTC Tang Scholar" program, and the Fundamental Research Funds for the Central Universities (KY2080000063). We also acknowledge the entire Van Allen Probes instrument teams and the OMNI database provided by NASA.

References

Araki, T., Fujitani, S., Emoto, M., Yumoto, K., Shiokawa, K., Ichinose, T., et al. (1997). Anomalous sudden commencement on March 24, 1991. *Journal of Geophysical Research*, *102*(A7), 14075–14086. https://doi.org/10.1029/96JA03637

Araki, T., Funato, K., Iguchi, T., & Kamei, T. (1993). Direct detection of solar wind dynamic pressure effect on ground geomagnetic field. *Geophysical Research Letters*, *20*(9), 775–778. https://doi.org/10.1029/93GL00852

Blake, J. B., Kolasinski, W. A., Fillius, R. W., & Mullen, E. G. (1992). Injection of electrons and protons with energies of tens of MeV into L < 3 on March 24, 1991. *Geophysical Research Letters*, *19*(8), 821–824. https://doi.org/10.1029/92GL00624

Cattell, C., Breneman, A., Colpitts, C., Dombeck, J., Thaller, S., Tian, S., et al. (2017). Dayside response of the magnetosphere to a small shock compression: Van Allen Probes, Magnetospheric MultiScale, and GOES-13. *Geophysical Research Letters*, *44*(17), 8712–8720. https://doi.org/10.1002/2017GL074895

Chapman, S., & Ferraro, V. C. A. (1931). A new theory of magnetic storms. *Terrestrial Magnetism and Atmospheric Electricity*, *36*(2), 77–97. https://doi.org/10.1029/TE036i002p00077

Cohen, I. J., Mauk, B. H., Turner, D. L., Fennell, J. F., Blake, J. B., Reeves, G. D., et al. (2019). Drift-dispersed flux dropouts of energetic electrons observed in Earth's middle magnetosphere by the Magnetospheric Multiscale (MMS) mission. *Geophysical Research Letters*, *46*(6), 3069–3078. https://doi.org/10.1029/2019GL082008

Fathy, A., Kim, K.-H., Park, J.-S., Jin, H., Kletzing, C., Wygant, J. R., & Ghamry, E. (2018). Characteristics of sudden commencements observed by Van Allen Probes in the inner magnetosphere. *Journal of Geophysical Research: Space Physics*, *123*(2), 1295–1304. https://doi.org/10.1002/2017JA024770

Foster, J. C., Wygant, J. R., Hudson, M. K., Boyd, A. J., Baker, D. N., Erickson, P. J., & Spence, H. E. (2015). Shock-induced prompt relativistic electron acceleration in the inner magnetosphere. *Journal of Geophysical Research: Space Physics*, *120*(3), 1661–1674. https://doi.org/10.1002/2014JA020642

Fu, H. S., Cao, J. B., Mozer, F. S., Lu, H. Y., & Yang, B. (2012). Chorus intensification in response to interplanetary shock. *Journal of Geophysical Research*, *117*(A1), A01203. https://doi.org/10.1029/2011JA016913

Hao, Y. X., Zong, Q., Zhou, X., Fu, S. Y., Rankin, R., Yuan, C., et al. (2016). Electron dropout echoes induced by interplanetary shock: Van Allen Probes observations. *Geophysical Research Letters*, *43*(11), 5597–5605. https://doi.org/10.1002/2016GL069140

Jin, Y., Liu, N., Su, Z., Zheng, H., Wang, Y., & Wang, S. (2022). Immediate impact of solar wind dynamic pressure pulses on whistler-mode chorus waves in the inner magnetosphere. *Geophysical Research Letters*, *49*(5), e2022GL097941. https://doi.org/10.1029/2022GL097941

Kan, J. R. (1990). Tail-like reconfiguration of the plasma sheet during the substorm growth phase. *Geophysical Research Letters*, *17*(13), 2309–2312. https://doi.org/10.1029/GL017i013p02309

Kanekal, S. G., Baker, D. N., Fennell, J. F., Jones, A., Schiller, Q., Richardson, I. G., et al. (2016). Prompt acceleration of magnetospheric electrons to ultrarelativistic energies by the 17 March 2015 interplanetary shock. *Journal of Geophysical Research: Space Physics*, *121*(8), 7622–7635. https://doi.org/10.1002/2016JA022596

Kim, K.-H., Lee, D., Shiokawa, K., Lee, E., Park, J., Kwon, H., et al. (2012). Magnetospheric responses to the passage of the interplanetary shock on 24 November 2008. *Journal of Geophysical Research*, *117*(A10), A10209. https://doi.org/10.1029/2012JA017871

Kim, K.-H., Park, K. S., Ogino, T., Lee, D.-H., Sung, S.-K., & Kwak, Y.-S. (2009). Global MHD simulation of the geomagnetic sudden commencement on 21 October 1999. *Journal of Geophysical Research*, *114*(A8), A08212. https://doi.org/10.1029/2009JA014109

Kletzing, C. A., Kurth, W. S., Acuna, M., MacDowall, R. J., Torbert, R. B., Averkamp, T., et al. (2013). The electric and magnetic field instrument suite and integrated science (EMFISIS) on RBSP. *Space Science Reviews*, *179*(1–4), 127–181. https://doi.org/10.1007/s11214-013-9993-6

Knott, K., Pedersen, A., & Wedeken, U. (1985). GEOS 2 electric field observations during a sudden commencement and subsequent substorms. *Journal of Geophysical Research*, *90*(A2), 1283–1288. https://doi.org/10.1029/JA090iA02p01283

Lee, D.-Y., & Lyons, L. R. (2004). Geosynchronous magnetic field response to solar wind dynamic pressure pulse. *Journal of Geophysical Research*, *109*(A4), A04201. https://doi.org/10.1029/2003JA010076

Liu, N., Su, Z., Gao, Z., Reeves, G. D., Zheng, H., Wang, Y., & Wang, S. (2017). Shock-induced disappearance and subsequent recovery of plasmaspheric hiss: Coordinated observations of RBSP, THEMIS, and POES satellites. *Journal of Geophysical Research: Space Physics*, *122*(10), 10421–10435. https://doi.org/10.1002/2017JA024470

Liu, N., Su, Z., Zheng, H., Wang, Y., & Wang, S. (2018). Prompt disappearance and emergence of radiation belt magnetosonic waves induced by solar wind dynamic pressure variations. *Geophysical Research Letters*, *45*(2), 585–594. https://doi.org/10.1002/2017GL076382

Liu, Y., Zong, Q.-G., Zhou, X.-Z., Hao, Y.-X., & Liu, Z.-Y. (2019). Understanding electron dropout echoes induced by interplanetary shocks: Test particle simulations. *Journal of Geophysical Research: Space Physics*, *124*(8), 6759–6775. https://doi.org/10.1029/2019JA027018

Liu, Z. Y., Zong, Q.-G., Hao, Y. X., Zhou, X.-Z., Ma, X. H., & Liu, Y. (2017). Electron dropout echoes induced by interplanetary shock: A statistical study. *Journal of Geophysical Research: Space Physics*, *122*(8), 8037–8050. https://doi.org/10.1002/2017JA024045

Ma, X.-H., Zong, Q.-G., Yue, C., Hao, Y.-X., & Liu, Y. (2021). Energetic electron enhancement and dropout echoes induced by solar wind dynamic pressure decrease: The effect of phase space density profile. *Journal of Geophysical Research: Space Physics*, *126*(3), e2020JA028863. https://doi.org/10.1029/2020JA028863

McIlwain, C. E. (1961). Coordinates for mapping the distribution of magnetically trapped particles. *Journal of Geophysical Research*, *66*(11), 3681–3691. https://doi.org/10.1029/JZ066i011p03681

Nishimura, Y., Kikuchi, T., Ebihara, Y., Yoshikawa, A., Imajo, S., Li, W., & Utada, H. (2016). Evolution of the current system during solar wind pressure pulses based on aurora and magnetometer observations. *Earth Planets and Space*, *68*(1), 144. https://doi.org/10.1186/s40623-016-0517-y

Samsonov, A. A., Sibeck, D. G., & Yu, Y. (2010). Transient changes in magnetospheric ionospheric currents caused by the passage of an interplanetary shock: Northward interplanetary magnetic field case. *Journal of Geophysical Research*, *115*(A5), A05207. https://doi.org/10.1029/2009JA014751

Schiller, Q., Kanekal, S. G., Jian, L. K., Li, X., Jones, A., Baker, D. N., et al. (2016). Prompt injections of highly relativistic electrons induced by interplanetary shocks: A statistical study of Van Allen Probes observations. *Geophysical Research Letters*, *43*(24), 12317–12324. https://doi.org/10.1002/2016GL071628

Shinbori, A., Ono, T., Iizima, M., & Kumamoto, A. (2004). SC related electric and magnetic field phenomena observed by the Akebono satellite inside the plasmasphere. *Earth Planets and Space*, *56*(2), 269–282. https://doi.org/10.1186/BF03353409

Sibeck, D. G., Lopez, R. E., & Roelof, E. C. (1991). Solar wind control of the magnetopause shape, location, and motion. *Journal of Geophysical Research*, *96*(A4), 5489–5495. https://doi.org/10.1029/90JA02464

Spence, H. E., Reeves, G. D., Baker, D. N., Blake, J. B., Bolton, M., Bourdarie, S., et al. (2013). Science goals and overview of the energetic particle, composition, and thermal plasma (ECT) suite on NASA's Radiation Belt Storm Probes (RBSP) mission. *Space Science Reviews*, *179*(1–4), 311–336. https://doi.org/10.1007/s11214-013-0007-5

Sun, T. R., Wang, C., Li, H., & Guo, X. C. (2011). Nightside geosynchronous magnetic field response to interplanetary shocks: Model results. *Journal of Geophysical Research*, *116*(A4), A04216. https://doi.org/10.1029/2010JA016074

Takahashi, N., Kasaba, Y., Nishimura, Y., Shinbori, A., Kikuchi, T., Hori, T., et al. (2017). Propagation and evolution of electric fields associated with solar wind pressure pulses based on spacecraft and ground-based observations. *Journal of Geophysical Research: Space Physics*, *122*(8), 8446–8461. https://doi.org/10.1002/2017JA023990

Tsurutani, B. T., & Lakhina, G. S. (2014). An extreme coronal mass ejection and consequences for the magnetosphere and Earth. *Geophysical Research Letters*, *41*(2), 287–292. https://doi.org/10.1002/2013GL058825

Tsurutani, B. T., Lakhina, G. S., Verkhoglyadova, O. P., Gonzalez, W. D., Echer, E., & Guarnieri, F. L. (2011). A review of interplanetary discontinuities and their geomagnetic effects. *Journal of Atmospheric and Solar-Terrestrial Physics*, *73*(1), 5–19. https://doi.org/10.1016/j.jastp.2010.04.001

Tsyganenko, N. A. (1989). A magnetospheric magnetic field model with a warped tail current sheet. *Planetary and Space Science*, *37*(1), 5–20. https://doi.org/10.1016/0032-0633(89)90066-4

Turner, D. L., Angelopoulos, V., Shprits, Y., Kellerman, A., Cruce, P., & Larson, D. (2012). Radial distributions of equatorial phase space density for outer radiation belt electrons. *Geophysical Research Letters*, *39*(9), L09101. https://doi.org/10.1029/2012GL051722

Usanova, M. E., Mann, I. R., Rae, I. J., Kale, Z. C., Angelopoulos, V., Bonnell, J. W., et al. (2008). Multipoint observations of magnetospheric compression-related EMIC Pc1 waves by THEMIS and CARISMA. *Geophysical Research Letters*, *35*(17), L17S25. https://doi.org/10.1029/2008GL034458

Wang, C., Liu, J. B., Li, H., Huang, Z. H., Richardson, J. D., & Kan, J. R. (2009). Geospace magnetic field responses to interplanetary shocks. *Journal of Geophysical Research*, *114*(A5), A05211. https://doi.org/10.1029/2008JA013794

Wygant, J., Bonnell, J. W., Goetz, K., Ergun, R. E., Mozer, F. S., Bale, S. D., et al. (2013). The electric field and waves instruments on the radiation belt storm probes mission. *Space Science Reviews*, *179*(1–4), 183–220. https://doi.org/10.1007/s11214-013-0013-7

Wygant, J., Mozer, F., Temerin, M., Blake, J., Maynard, N., Singer, H., & Smiddy, M. (1994). Large amplitude electric and magnetic field signatures in the inner magnetosphere during injection of 15 MeV electron drift echoes. *Geophysical Research Letters*, *21*(16), 1739–1742. https://doi.org/10.1029/94GL00375

Zesta, E., Singer, H. J., Lummerzheim, D., Russell, C. T., Lyons, L. R., & Brittnacher, M. J. (2000). The effect of the January 10, 1997, pressure pulse on the magnetosphere-ionosphere current system. In S.-I. Ohtani, R. Fujii, M. Hesse, & R. L. Lysak (Eds.), *Magnetospheric current systems*. https://doi.org/10.1029/GM118p0217

Zhang, D., Liu, W., Du, J., Yu, Y., Li, X., Sarris, T. E., & Cao, J. (2022). Response of electric field in terrestrial magnetosphere to interplanetary shock. *The Astrophysical Journal*, *938*(1), 70. https://doi.org/10.3847/1538-4357/ac90cc

Zhang, D., Liu, W., Li, X., Sarris, T., Xiao, C., & Wygant, J. R. (2018). Observations of impulsive electric fields induced by interplanetary shock. *Geophysical Research Letters*, *45*(15), 7287–7296. https://doi.org/10.1029/2018GL078809

Zhang, D., Liu, W., Li, X., Sarris, T. E., Hao, Y., & Zhang, Z. (2024). Surfing acceleration of radiation belt relativistic electrons induced by the propagation of interplanetary shock. *Geophysical Research Letters*, *51*(12), e2024GL109285. https://doi.org/10.1029/2024GL109285

Zhou, X., & Tsurutani, B. T. (1999). Rapid intensification and propagation of the dayside aurora: Large scale interplanetary pressure pulses (fast shocks). *Geophysical Research Letters*, *26*(8), 1097–1100. https://doi.org/10.1029/1999GL900173

Zuo, P., Feng, X., Xie, Y., Wang, Y., & Xu, X. (2015). Strong solar wind dynamic pressure pulses: Interplanetary sources and their impacts on geosynchronous magnetic fields. *The Astrophysical Journal*, *812*(2), 152–160. https://doi.org/10.1088/0004-637X/812/2/152